Inorganic Chemistry Cite This: Inorg. Chem. 2019, 58, 13737–13741

pubs.acs.org/IC

Photoinduced Terminal Hydride of [FeFe]-Hydrogenase Biomimetic **Complexes**

Scheme 1

Shuqiang Niu,[†] Anne E. Nelson,[‡] Patricia De La Torre,[‡] Haixia Li,[†] Carmen F. Works,*,[‡] and Michael B. Hall*,†

Supporting Information

ABSTRACT: The active site of the [FeFe]-hydrogenase ([FeFe]-H₂ase) has a bridging carbonyl ligand and a terminal hydride in the key H-cluster intermediate H_{hyd}. However, nearly all of the synthetic mimics reported, so far, prefer a hydride bridging the two irons, and only few mimics with a terminal hydride were achieved by tuning the steric effects of bulky diphosphine ligands. Moreover, although intermediates with either a terminal hydride or a protonated bridging thiolate ligand were proposed to exist during protonation processes or hydrogen exchange in the [FeFe]-H₂ase mimic, $[Fe_2(\mu-pdt)(\mu-H)(CO)_4(PMe_3)_2]^+$ (1H⁺), only bridging hydrides were observed by timeresolved IR spectroscopy. In this report, FTIR spectroscopy of 1H+, under CO with longer irradiation time, revealed several new photoinduced species. In addition to the CO loss species, many of the photoinduced products can be assigned to 1H+ with a terminal hydride by comparison of their CO vibrational frequencies with density functional theory calculations.

 $^{
m 7}$ he [FeFe]-hydrogenases ([FeFe]- ${
m H}_2$ ase) catalyze the reversible conversion between H2 and protons/electrons under mild conditions.1-4 In particular, a protonated intermediate of the H-cluster, H_{hvd}, with a terminal apical hydride at an iron site has been recognized as a key in the enzyme's hydrogen evolving reaction along a heterolytic reaction pathway (Scheme 1). S-10 Thus, such terminal hydride species are prime targets for synthetic efforts in biomimetic complexes and artificial enzymes. 11-13 However, in most of the synthetic mimics reported so far, the hydride prefers a bridging site between the two irons due to its higher stability, 14-16 which leads to a less active site for H₂ production (Scheme 1), 11 and only few [FeFe]-H2ase active site mimics bearing a terminal hydride were achieved and characterized by tuning steric effects of the bulk diphosphine ligands because of limited thermal stability. 17,18 After the light-driven H/D exchange of [Fe2(µ $pdt)(\mu-H)(CO)_4(PMe_3)_2]^+ (1H^+) (pdt = S_2C_3H_6, PMe_3 =$ trimethylphosphine) to $1D^+$ was reported, 14,19 photochemical H₂ production with [FeFe]-H₂ase mimics has made significant progress. 11,20-23 However, due to the complexity of photochemical reactions, little is known about the catalytically active site induced by light in these biomimetic model complexes. Although recent computational studies of the electronically excited states suggested that CO loss might be less favored than

Cys////, CO $\mathbf{H}_{\mathrm{hyd}}$ $L = CO, CN, PR_3$ **Biomimetic Model** [FeFe]H₂ase active site H^{+} CO

Fe-S bond cleavage,²⁴ more recent experimental results strongly support CO loss as the dominant photochemical process.²⁵ Here, we report our findings that photolysis in the presence of CO produces a photoinduced 1H+ species with a terminal apical hydride.

The 1H+ samples were prepared 19 and collected using a gastight, sealed IR cell (International Crystal Laboratories) with CaF₂ windows (path length 0.2 mm) and were photolyzed directly in the cell using a hand-held Hg lamp with a short wavelength of 254 nm and a long wavelength of 365 nm. A typical photolysis protocol had continuous exposure in 5 min intervals over the course of 25 min. Spectra were collected immediately following each photolysis interval and/or at regular intervals post-photolysis to monitor thermal changes. Spinunrestricted density functional theory (DFT) calculations with the M06 density functional and Dgauss DZVP2 basis sets were carried out for the structure, energy, and CO vibrational frequencies of excitation states along possible photochemical reactions (computational details in the Supporting Informa-

The relative positions of two PMe₃ ligands and the folding direction of the pdt ligand in the complex [1H+] (the

Received: June 14, 2019 Published: September 30, 2019



Department of Chemistry, Texas A&M University, College Station, Texas 77843-3255, United States

^{*}Department of Chemistry, Sonoma State University, Rohnert Park, California 94928, United States

parentheses refer to all isomers of this species) result in five fluxional isomers with a bridging hydride ([$1H_b^+$]): $1aH_b^+$ (trans-basal/basal isomer), $1bH_b^+$ (cis-basal/basal), $1cH_b^+$ (apical/basal), $1dH_b^+$ (basal/apical), and $1eH_b^+$ (apical/apical) (Scheme S1). The IR spectrum of [$1H^+$] shows two characteristic CO vibrational absorption bands ($\nu_{\rm CO}$) at 1990 and 2032 cm⁻¹ as well as a weak shoulder band at 2046 cm⁻¹ in dichloromethane (DCM) (Figure S1a, Tables 1 and S1). The DFT $\nu_{\rm CO}$ calculations reveal that the [$1H_b^+$] in the DCM is a mixture of the most stable isomers $1aH_b^+$ and $1cH_b^+$ and possibly some $1bH_b^+$ (Figure 1).

Table 1. M06/DZVP2 Calculated Relative Energies $\Delta E_{\rm e}$ (kcal/mol) in DCM and CO Vibrational Frequencies ($\nu_{\rm CO}$ cm $^{-1}$) of the [1H $^+$], Most Likely Photoproducts of [1H $^+$], and [4H $^+$]

ΔE	$ u_{\mathrm{CO}}^{-1}$	ν_{CO}^{2}	$ u_{\rm CO}^{3}$	ν_{CO}^{-4}	intensity
$[1H_b^+]$					
0.00	1995	1997	2019	2037	m,m,s,vw
3.40	2002	2006	2030	2048	m,m,m,m
4.44	1999	2005	2034	2048	m,m,m,m
	1900	1900	2032	2046	m,m,s,vw
Photoproducts					
17.98	1920	2011	2040	2051	w,m,m,m
18.47	1948	2014	2036	2048	w,m,m,m
17.20	1889	2010	2016	2041	m,m,m,w
30.56	1943	1958	1991	2004	m,m,s,vw
28.89	1956	1974	1988	2018	m,w,s,m
40.90	1954	1961	1997	2006	m,s,m,m
43.06	2000	2005	2037		m,m,m
40.22	2005	2006	2036		m,m,w
56.61	1940	2027	2040		w,m,m
	1944	1977	2017	2050	
$[4\mathrm{H}^+]$					
0.00	1949	1955			m,w
	1928	1940			
14.22	1862	1963			w,m
	1874	1940			
	0.00 3.40 4.44 17.98 18.47 17.20 30.56 28.89 40.90 43.06 40.22 56.61	0.00 1995 3.40 2002 4.44 1999 1900 Phot 17.98 1920 18.47 1948 17.20 1889 30.56 1943 28.89 1956 40.90 1954 43.06 2000 40.22 2005 56.61 1940 1944 0.00 1949 1928 14.22 1862		$ \begin{array}{c ccccccccccccccccccccccccccccccccccc$	$ \begin{array}{c ccccccccccccccccccccccccccccccccccc$

^aIn DCM solution. ^bIn DCM (N₂). ^cIn MeCN solution. ²⁶

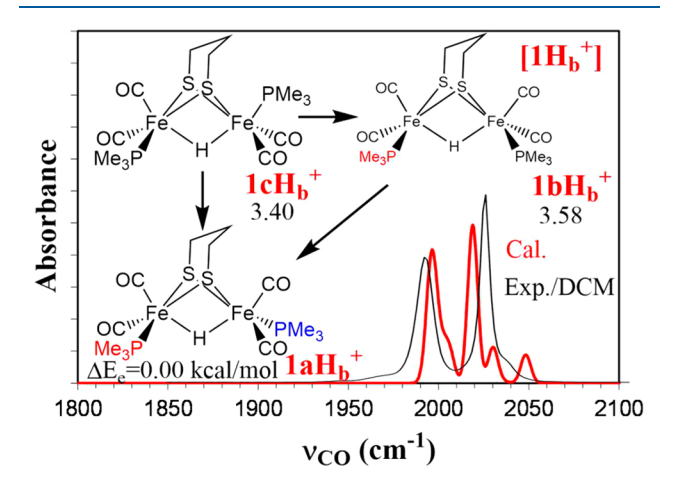


Figure 1. DFT simulated IR spectrum and relative energies $\Delta E_{\rm e}$ (in DCM, kcal/mol) of $[{\bf 1H_b}^+]$ with isomers ${\bf 1aH_b}^+$ at 80% and ${\bf 1cH_b}^+/$ ${\bf 1bH_b}^+$ at 20% in DCM (calculated: red; experimental: black). The individual DFT simulated IR spectra of ${\bf 1aH_b}^+$, ${\bf 1cH_b}^+$, and ${\bf 1bH_b}^+$ are shown in Figure S1a.

As observed by FTIR spectroscopy in the DCM solution under N_2 (Figure 2a), irradiations at the minute time scale

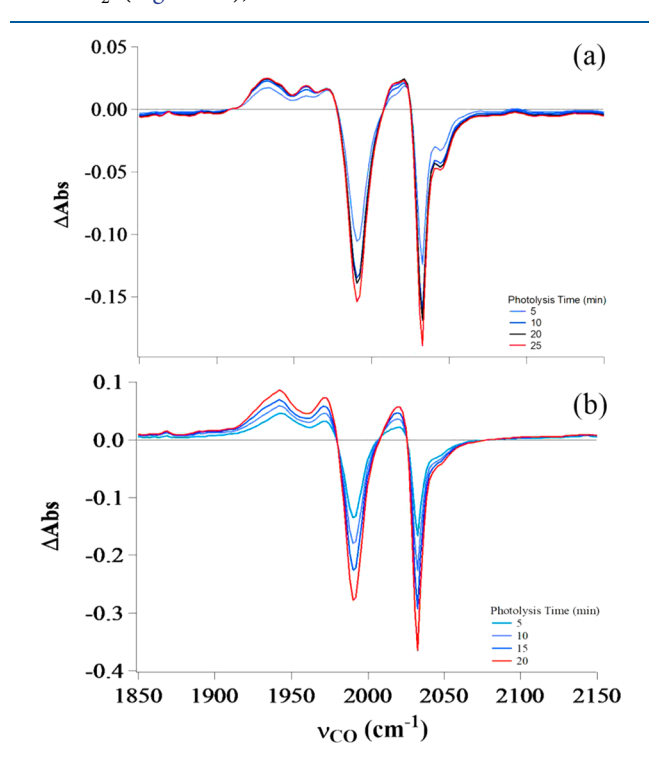
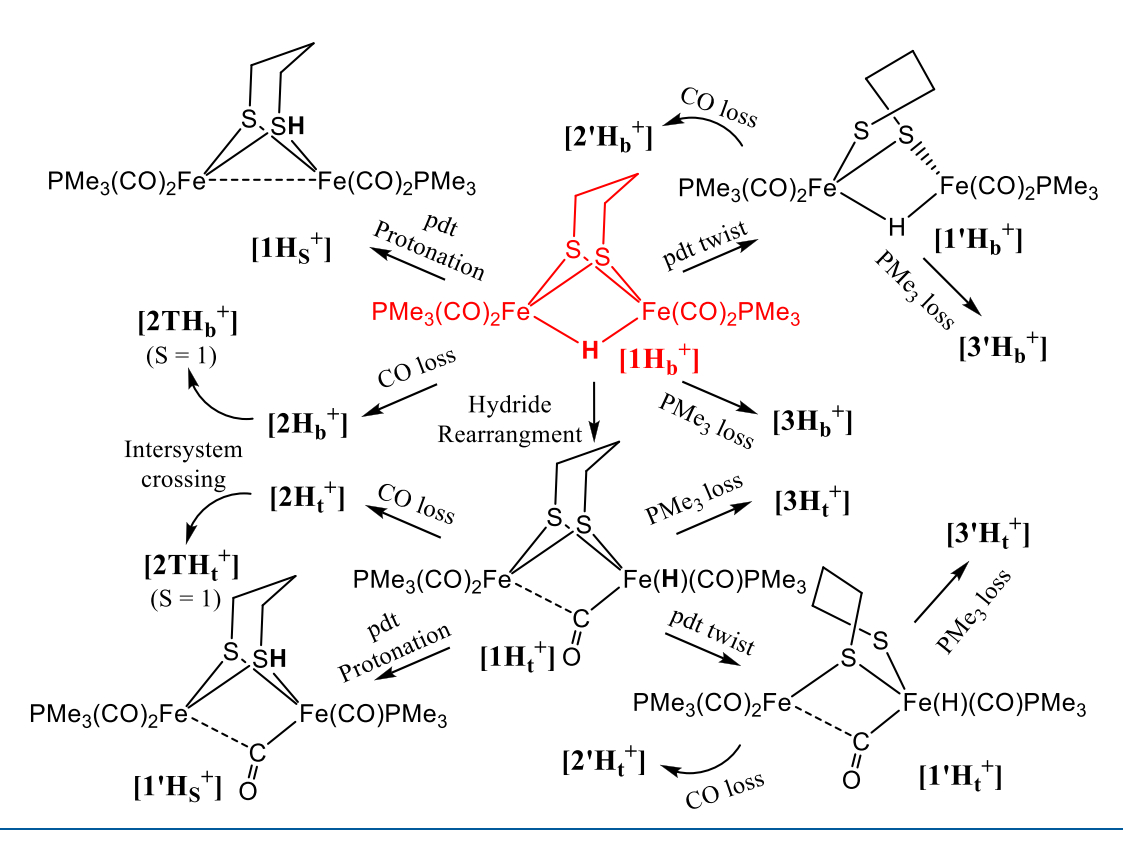


Figure 2. Spectral changes in the IR of $1H^+$ upon photolysis with 365 nm light shown as difference spectra in 5 min intervals, (a) $1H^+$ in DCM under nitrogen and (b) $1H^+$ in DCM under CO.

produce strong bleaching of the ν_{CO} peaks of the parent $[1H_b^+]$ at 1990, 2032, and 2048 cm⁻¹ and growth of new ν_{CO} peaks at 1932, 1958, 1972, and 2020 cm⁻¹. The CO loss of 1H⁺ was confirmed by qualitative CO detection using spectral changes of the Rh-dimer in DCM during 365 nm of photolysis. It is noteworthy that, in DCM under CO, the bleach of the parent $\nu_{\rm CO}$ peak at 2050 cm⁻¹ and the growth peak at 1958 cm⁻¹ are reduced with the growth of the new $\nu_{\rm CO}$ peaks at 1942 and 1972 cm⁻¹ (Figure 2b). In particular, the bleach of the parent $\nu_{\rm CO}$ peaks at 1990 and 2032 cm⁻¹ under CO (Figure 2b) doubly increase under irradiation above 20 min with respect to those in the DCM solution under N₂ (Figure 2a). Since dissolved CO solutes may inhibit CO loss of $[1H_b^+]$, the variation in the $\nu_{\rm CO}$ peak at ~2050 cm⁻¹ and lack of peak at 1958 cm⁻¹ and the continuous growth of the $\nu_{\rm CO}$ peaks at 1942 and 1972 cm⁻¹ implicate the presence of a new photoproduced species in addition to the CO loss species.

The new photoinduced species can be probed by the DFT calculations of possible photochemical reactions of $[1H^+]$, including deprotonation, intersystem crossing between the singlet and triplet states, hydride rearrangement, pdt ligand protonation (proton transfer to S), pdt ligand twist (including possible Fe–S bond cleavage), CO loss, and PMe₃ as well as hydride dissociation (Scheme 2). Of these possible reactions, the hydride rearrangement to species with a terminal hydride and a half-bridging CO $[1H_t^+]$ appears to be energetically favorable, in agreement with a previous study, ¹⁶ and to have $\nu_{\rm CO}$ bands consistent with the new observations. In other words, when the CO loss species reattaches a CO from solution, the most stable species other than the parent is $[1H_t^+]$. The most stable isomers of $[1H_t^+]$ $(1a3H_t^+, 1c3H_t^+,$ and $1c4H_t^+)$ exhibit

Scheme 2



three $\nu_{\rm CO}$ bands at 1890–1950, ~2010, and 2041–2051 cm⁻¹ (Figure S1b, Tables 1 and S1). Consequently, the hydride rearrangement of [1H_b⁺] to [1H_t⁺] can give rise to growth of peaks at 1890-1950 (exp. 1943) and 2010 (exp. 2020) cm⁻¹ and decrease in the parent peak at $\sim 2030 \text{ cm}^{-1}$ (exp. 2046 cm⁻¹) as well as result some slight changes in the range of 2036-2051 cm⁻¹ (Figure 3a). Remarkably, the variations in the IR spectrum from $[1H_h^+]$ to $[1H_t^+]$ (Figure S1b) are consistent with those of a pair of biomimetic model complexes, $[Fe_2(\mu\text{-edt})(\mu\text{-H})$ - $(CO)_2(PMe_3)_4]^+$ (4H_b⁺) with a bridging hydride and [Fe₂(μ $edt)(t-H)(CO)_2(PMe_3)_4]^+$ with a terminal hydride $(4H_t^+)$ (Figure S2), which were synthesized and fully characterized by crystallography, NMR, and IR.²⁶ In particular, 4H_t⁺ liberates H₂ upon treatment with the strong acids. Notably, the M06/ DZVP2 optimized geometry of 4H_t⁺ shows a half-bridging CO, which binds to the hydridic iron center and is in agreement with the reported X-ray crystal structure. Moreover, a comparison of the two ν_{CO} bands of $4H_h^+$ (calc. 1949 and 1955 cm⁻¹; exp. 1928 and 1940 cm⁻¹) with those of $4H_t^+$ (calc. 1862 and 1963 cm⁻¹; exp. 1874 and 1940 cm⁻¹) shows a dramatic redshift in the low energy band from $4H_b^+$ to $4H_t^+$ (calc. 87 cm⁻¹; exp. 54 cm⁻¹) (Figure S2 and Table 1). This redshift is almost identical to the redshift here for the corresponding band from $[1H_h^+]$ to $[1H_h^+]$ (calc. 76 cm⁻¹; exp. 48 cm⁻¹) (Table 1). Thus, the observed photoproducts showing growth of $\nu_{\rm CO}$ peaks at 1944 and 1977 cm⁻¹ from photolysis of [1H⁺] under CO appear to be terminal hydride species.

Furthermore, among the possible isomers with a CO loss, $[2H_b^+]$, $[2H_t^+]$, $[2'H_b^+]$, and $[2'H_t^+]$ (Schemes 2 and S2), the most stable CO loss species $2aT2H_b^+$ and $2aT4H_b^+$ (T indicates a triplet state) exhibit two $\nu_{\rm CO}$ bands at ~2004 and 2037 cm⁻¹, while the species with a bridging CO and a terminal hydride ($[2H_t^+]$), $2aT3bH_t^+$, $2aT3cH_t^+$, and $2aT3dH_t^+$, show two typical $\nu_{\rm CO}$ bands at 1887-1940 (exp. 1960-1972 cm⁻¹) and

2040–2049 cm $^{-1}$ (exp. 2020–2046 cm $^{-1}$) (Figure S1c, Tables 1 and S2). Thus, the DFT calculations reveal that the added CO in the photolysis of $1H^+$ is clearly implicated in the growth peaks at $1890-1950~{\rm cm}^{-1}$ and leads to the recovery of the parent peaks (Figure 3b), especially under N_2 .

Moreover, species with protonation on a sulfur, $[1H_S^+]$, were suggested as an intermediate in the conversion between $[1H_h^{+}]$ and [1H_t⁺]. B DFT calculations show that the most stable species of $[1H_S^+]$ and $[1'H_S^+]$ (Scheme S1), $1a6H_S^+$, $1c6H_S^+$, and $1aT7H_S^+$, give rise to the growth of ν_{CO} peaks at 1922-1977, ~1990, and 2004-2018 cm⁻¹, red-shifted due to the reduction of the iron centers (Figure S1d, Tables 1 and S2). Since these spectral features are similar to those of $[1H_t^+]$ except for the stronger intensity of the $\nu_{\rm CO}$ peaks at ~1990 cm⁻¹ (Figure 3c), we further looked carefully for the $\nu_{\rm SH}$ at ~2550 cm⁻¹ in the experiment (Figure S3b) and found no certain evidence for the presence of this species. Moreover, other species produced along the photochemical reaction pathways of the deprotonation, intersystem crossing, pdt twist, and PMe₃ or hydride loss can be excluded from photoproducts observed because of either their poor stability or their mismatched $\nu_{\rm CO}$ bands with respect to the experimental ν_{CO} bands (Schemes S1 and S2 and Tables S1-S3). Overall, our DFT calculations suggest that in addition to the CO loss species the observed species with the growth $\nu_{\rm CO}$ peaks at 1942, 1972, and 2020 cm⁻¹ for 1H⁺ should mainly correspond to the species with a terminal hydride (Table 1).

In summary, biomimetic model complexes of [FeFe]- H_2 ase active sites with either terminal hydride or protonated thiolate bridging ligand may play an important role in H_2 production and hydrogen exchange processes. Photochemistry provides a fresh way to promote catalytic activity of these mimics. Under irradiation at a minute time scale, a hydride rearrangement from a species with a bridging hydride to a species with a terminal

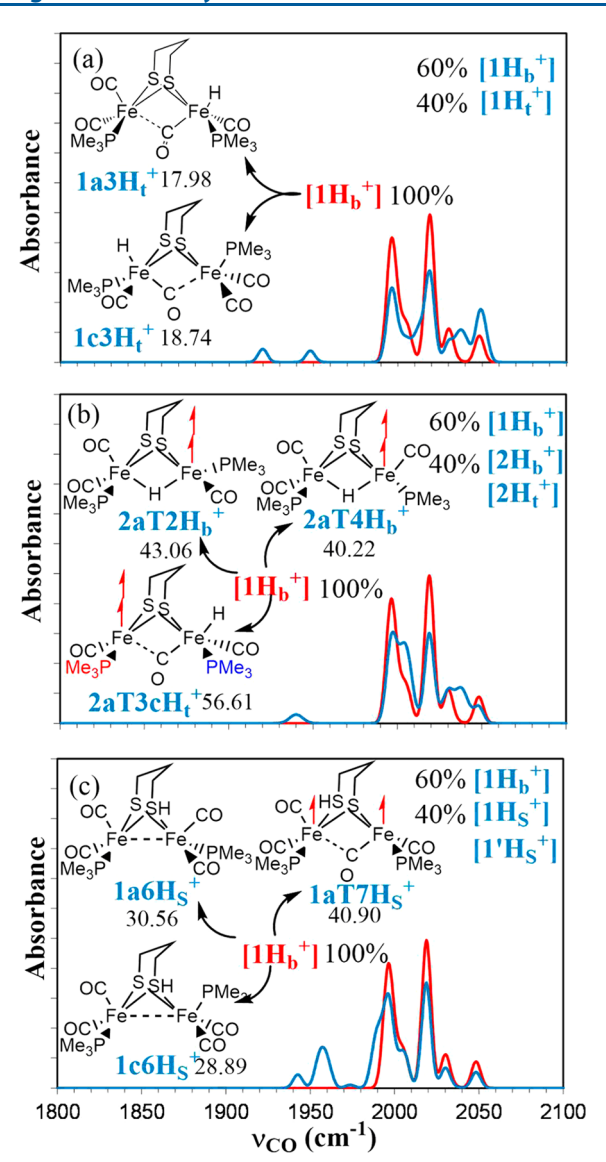


Figure 3. DFT simulated IR spectrum and relative energies to $1a\mathbf{H}_b^+$ ΔE_e (in DCM, kcal/mol) of the possible photochemical products: (a) the hydride rearrangement isomers with a terminal hydride $[1\mathbf{H}_t^+]$ at 40% and $[1\mathbf{H}_b^+]$ at 60% (blue); (b) the CO loss isomers $[2\mathbf{H}_b^+]$ and $[2\mathbf{H}_t^+]$ at 40% and $[1\mathbf{H}_b^+]$ at 60% (blue); (c) the protonated-pdt isomers $[1\mathbf{H}_S^+]$ and $[1'\mathbf{H}_S^+]$ at 40% and $[1\mathbf{H}_b^+]$ at 60% (blue). The spectra of the parent $[1\mathbf{H}_b^+]$ at 100% are in red. The small arrow represents an unpaired electron. The individual DFT simulated IR spectra of these species are shown in Figure S1b,c.

hydride can be easily achieved in addition to CO ligand loss. The methodology combining experimental spectroscopies with a DFT aided assignment could be applicable to probe the stability and activity of the [FeFe]- H_2 ase active site mimics for hydrogen evolution under light.

ASSOCIATED CONTENT

S Supporting Information

The Supporting Information is available free of charge on the ACS Publications website at DOI: 10.1021/acs.inorg-chem.9b01738.

Detailed computational methods, experimental and calculated relative energies and vibrational frequencies, IR spectra, and relative energies (PDF)

AUTHOR INFORMATION

Corresponding Authors

*E-mail: hall@science.tamu.edu. *E-mail: works@sonoma.edu.

ORCID ®

Shuqiang Niu: 0000-0001-9355-3007 Michael B. Hall: 0000-0003-3263-3219

Notes

The authors declare no competing financial interest.

ACKNOWLEDGMENTS

This work was supported by the National Science Foundation (CFW CHE-1664609 and MBH CHE-1664866). The Texas A&M University Supercomputing Facility is acknowledged for providing computing resources. The NWChem calculations were partially performed at the Environmental Molecular Sciences Laboratory (EMSL), a national user facility sponsored by the U.S. DOE's Office of Biological and Environmental Research and located at Pacific Northwest National Laboratory, operated for DOE by Battelle, under the grant EMSL 48430.

REFERENCES

- (1) Fontecilla-Camps, J. C.; Volbeda, A.; Cavazza, C.; Nicolet, Y. Structure/Function Relationships of [NiFe]- and [FeFe]-Hydrogenases. *Chem. Rev.* **2007**, *107*, 4273–4303.
- (2) Lubitz, W.; Ogata, H.; Ruediger, O.; Reijerse, E. Hydrogenases. *Chem. Rev.* **2014**, *114*, 4081–4148.
- (3) Peters, J. W.; Schut, G. J.; Boyd, E. S.; Mulder, D. W.; Shepard, E. M.; Broderick, J. B.; King, P. W.; Adams, M. W. W. [FeFe]- and [NiFe]-Hydrogenase Diversity, Mechanism, and Maturation. *Biochim. Biophys. Acta, Mol. Cell Res.* **2015**, *1853*, 1350–1369.
- (4) Haumann, M.; Stripp, S. T. The Molecular Proceedings of Biological Hydrogen Turnover. Acc. Chem. Res. 2018, 51, 1755–1763.
- (5) Fan, H. J.; Hall, M. B. A Capable Bridging Ligand for Fe-only Hydrogenase: Density Functional Calculations of a Low-Energy Route for Heterolytic Cleavage and Formation of Dihydrogen. *J. Am. Chem. Soc.* **2001**, *123*, 3828–3829.
- (6) Siegbahn, P. E.; Tye, J. W.; Hall, M. B. Computational Studies of [NiFe] and [FeFe] Hydrogenases. *Chem. Rev.* **2007**, *107*, 4414–4435.
- (7) Rumpel, S.; Sommer, C.; Reijerse, E.; Fares, C.; Lubitz, W. Direct Detection of the Terminal Hydride Intermediate in [FeFe] Hydrogenase by NMR Spectroscopy. *J. Am. Chem. Soc.* **2018**, *140*, 3863–3866.
- (8) Reijerse, E. J.; Pham, C. C.; Pelmenschikov, V.; Gilbert-Wilson, R.; Adamska-Venkatesh, A.; Siebel, J. F.; Gee, L. B.; Yoda, Y.; Tamasaku, K.; Lubitz, W.; Rauchfuss, T. B.; Cramer, S. P. Direct Observation of an Iron-Bound Terminal Hydride in [FeFe]-Hydrogenase by Nuclear Resonance Vibrational Spectroscopy. *J. Am. Chem. Soc.* **2017**, *139*, 4306–4309.
- (9) Winkler, M.; Senger, M.; Duan, J. F.; Esselborn, J.; Wittkamp, F.; Hofmann, E.; Apfel, U. P.; Stripp, S. T.; Happe, T. Accumulating the Hydride State in the Catalytic Cycle of [FeFe]-Hydrogenases. *Nat. Commun.* **2017**, *8*, 7.
- (10) Pham, C. C.; Mulder, D. W.; Pelmenschikov, V.; King, P. W.; Ratzloff, M. W.; Wang, H.; Mishra, N.; Alp, E. E.; Zhao, J.; Hu, M. Y.; Tamasaku, K.; Yoda, Y.; Cramer, S. P. Terminal Hydride Species in [FeFe]-Hydrogenases Are Vibrationally Coupled to the Active Site Environment. *Angew. Chem., Int. Ed.* **2018**, *57*, 10605–10609.
- (11) Schilter, D.; Camara, J. M.; Huynh, M. T.; Hammes-Schiffer, S.; Rauchfuss, T. B. Hydrogenase Enzymes and Their Synthetic Models: The Role of Metal Hydrides. *Chem. Rev.* **2016**, *116*, 8693–8749.
- (12) Esselborn, J.; Lambertz, C.; Adamska-Venkatesh, A.; Simmons, T.; Berggren, G.; Noth, J.; Siebel, J.; Hemschemeier, A.; Artero, V.; Reijerse, E.; Fontecave, M.; Lubitz, W.; Happe, T. Spontaneous Activation of [FeFe]-Hydrogenases by an Inorganic [2Fe] Active Site Mimic. *Nat. Chem. Biol.* **2013**, *9*, 607–609.

(13) Esmieu, C.; Raleiras, P.; Berggren, G. From Protein Engineering to Artificial Enzymes - Biological and Biomimetic Approaches towards Sustainable Hydrogen Production. *Sustainable Energy & Fuels* **2018**, *2*, 724–750.

- (14) Zhao, X.; Georgakaki, I. P.; Miller, M. L.; Mejia-Rodriguez, R.; Chiang, C. Y.; Darensbourg, M. Y. Catalysis of H₂/D₂ Scrambling and Other H/D Exchange Processes by [Fe]-Hydrogenase Model Complexes. *Inorg. Chem.* **2002**, *41*, 3917–3928.
- (15) Wright, J. A.; Pickett, C. J. Protonation of a Subsite Analogue of [FeFe]-Hydrogenase: Mechanism of a Deceptively Simple Reaction Revealed by Time-Resolved IR Spectroscopy. *Chem. Commun.* (*Cambridge, U. K.*) **2009**, 5719–5721.
- (16) Liu, C. P.; Peck, J. N. T.; Wright, J. A.; Pickett, C. J.; Hall, M. B. Density Functional Calculations on Protonation of the FeFe-Hydrogenase Model Complex Fe₂(μ-pdt)(CO)₄(PMe₃)₂ and Subsequent Isomerization Pathways. *Eur. J. Inorg. Chem.* **2011**, 2011, 1080–1093.
- (17) Carroll, M. E.; Barton, B. E.; Rauchfuss, T. B.; Carroll, P. J. Synthetic Models for the Active Site of the [FeFe]-Hydrogenase: Catalytic Proton Reduction and the Structure of the Doubly Protonated Intermediate. J. Am. Chem. Soc. 2012, 134, 18843—18852.
- (18) Zaffaroni, R.; Rauchfuss, T. B.; Gray, D. L.; De Gioia, L.; Zampella, G. Terminal vs Bridging Hydrides of Diiron Dithiolates: Protonation of Fe₂(dithiolate)(CO)₂(PMe₃)₄. J. Am. Chem. Soc. **2012**, 134, 19260–19269.
- (19) Zhao, X.; Georgakaki, I. P.; Miller, M. L.; Yarbrough, J. C.; Darensbourg, M. Y. H/D Exchange Reaction in Dinuclear Iron Thiolates as Activity Assay Models of Fe- H_2 ase. *J. Am. Chem. Soc.* **2001**, 123, 9710–9711.
- (20) Wang, M.; Chen, L.; Li, X.; Sun, L. Approaches to Efficient Molecular Catalyst Systems for Photochemical $\rm H_2$ Production using [FeFe]-Hydrogenase Active Site Mimics. *Dalton Trans* **2011**, *40*, 12793–12800.
- (21) Junge, H.; Rockstroh, N.; Fischer, S.; Bruckner, A.; Ludwig, R.; Lochbrunner, S.; Kuhn, O.; Beller, M. Light to Hydrogen: Photocatalytic Hydrogen Generation from Water with Molecularly-Defined Iron Complexes. *Inorganics* **2017**, *5*, 14.
- (22) Lunsford, A. M.; Blank, J. H.; Moncho, S.; Haas, S. C.; Muhammad, S.; Brothers, E. N.; Darensbourg, M. Y.; Bengali, A. A. Catalysis and Mechanism of H₂ Release from Amine-Boranes by Diiron Complexes. *Inorg. Chem.* **2016**, *55*, 964–973.
- (23) Wang, W. G.; Rauchfuss, T. B.; Bertini, L.; Zampella, G. Unsensitized Photochemical Hydrogen Production Catalyzed by Diiron Hydrides. *J. Am. Chem. Soc.* **2012**, *134*, 4525–4528.
- (24) Bertini, L.; Fantucci, P.; De Gioia, L.; Zampella, G. Excited State Properties of Diiron Dithiolate Hydrides: Implications in the Unsensitized Photocatalysis of H₂ Evolution. *Inorg. Chem.* **2013**, *52*, 9826–9841.
- (25) Frederix, P.; Adamczyk, K.; Wright, J. A.; Tuttle, T.; Ulijn, R. V.; Pickett, C. J.; Hunt, N. T. Investigation of the Ultrafast Dynamics Occurring during Unsensitized Photocatalytic H₂ Evolution by an [FeFe]-Hydrogenase Subsite Analogue. *Organometallics* **2014**, *33*, 5888–5896.
- (26) van der Vlugt, J. I.; Rauchfuss, T. B.; Whaley, C. M.; Wilson, S. R. Characterization of a Diferrous Terminal Hydride Mechanistically Relevant to the Fe-only Hydrogenases. *J. Am. Chem. Soc.* **2005**, *127*, 16012–16013.